Dependence of Cavitation, Chemical Effect, and Mechanical Effect Thresholds on Ultrasonic Frequency

Tam Thanh Nguyen[a,b], Yoshiyuki Asakura[c], Shinobu Koda[d], Keiji Yasuda[a*]

[a]*Department of Chemical Engineering, Graduate School of Engineering, Nagoya University, Nagoya 464-8603, Japan*

[b]*Faculty of Environment, University of Science, VNU-HCM, Vietnam*

[c]*Honda Electronics Co., Ltd., Toyohashi, Aichi 441-3193, Japan*

[d]*Department of Molecular Design and Engineering, Graduate School of Engineering, Nagoya University, Nagoya 464-8603, Japan*

Email: yasuda@nuce.nagoya-u.ac.jp

Cavitation, chemical effect, and mechanical effect thresholds were investigated in wide frequency ranges from 22 to 4880 kHz. Each threshold was measured in terms of sound pressure at fundamental frequency. Broadband noise emitted from acoustic cavitation bubbles was detected by a hydrophone to determine the cavitation threshold. Potassium iodide oxidation caused by acoustic cavitation was used to quantify the chemical effect threshold. The ultrasonic erosion of aluminum foil was conducted to estimate the mechanical effect threshold. The cavitation, chemical effect, and mechanical effect thresholds increased with increasing frequency. The chemical effect threshold was close to the cavitation threshold for all frequencies. At low frequency below 98 kHz, the mechanical effect threshold was nearly equal to the cavitation threshold. However, the mechanical effect threshold was greatly higher than the cavitation threshold at high frequency. In addition, the thresholds of the second harmonic and the first ultraharmonic signals were measured to detect bubble occurrence. The threshold of the second harmonic approximated to the cavitation threshold below 1000 kHz. On the other hand, the threshold of the first ultraharmonic was higher than the cavitation threshold below 98 kHz and near to the cavitation threshold at high frequency.

Key words: cavitation threshold, broadband noise, potassium iodide, aluminum foil erosion, harmonic, ultraharmonic

1. Introduction

When ultrasound is irradiated to a liquid, tiny bubbles occur, oscillate, and collapse. This phenomenon is called acoustic cavitation. Acoustic cavitation produces high local pressure, temperature, and velocity fields in a liquid. Acoustic cavitation is applied widely in the various fields of industry such as ultrasonic cleaner, sonochemical reactor [1-4], homogenizer [5], atomizer [6], and food processing [7, 8]. However, there are some drawbacks of acoustic cavitation. In ultrasonic cleaning for semiconductor production in megahertz range, an extra amount of cavitation might cause severe damage on electric devices. In diagnostic medicine and therapy [9], cavitation might destroy normal cells in human bodies.

The cavitation threshold is defined as the minimum amplitude of sound pressure required to initiate acoustic cavitation. Investigations of cavitation threshold are of considerable importance for application of ultrasonic technologies in order to completely ensure the safety of objects and medium during irradiation. Until now, the cavitation threshold was measured by many methods such as broadband noise [10-15], acoustic emission [16-18], bubble observation [19], sonochemical luminescence [20], sonoluminescence [21], and aluminum foil erosion [22]. The effect associated with acoustic cavitation in a liquid comprises of chemical and mechanical effects which are powerful tools for industrial applications of ultrasound. Chemical effect arises from free radical production and pyrolysis owing to local high temperature and pressure [23-26]. Mechanical effect is principally generated by shockwaves and microjets with high velocity. The thresholds of chemical and mechanical effects should be seperatedly determined since their generation mechanisms are different.

The acoustic emission from bubbles under ultrasonic irradiation consists of harmonics (integer multiplies of fundamental), subharmonics (fundamental frequency divided by integer), ultraharmonics (integer multiples of subharmonics excepting the fundamental and harmonics), and broadband noise components. These frequency spectra are received by a hydrophone. Recently, broadband noise is generally used for the measurement of cavitation threshold because it is directly attributed to cavity collapse. The quantity of broadband noise is estimated by the broadband integrated voltage (BIV) which is an integration value of broadband noise [10-15]. Hodnett and Zeqiri irradiated ultrasound at 25 kHz and measured BIV in the frequency range of 1.5 - 8 MHz [12]. Uchida et al. used driving frequency at 150 kHz and measured BIV in the region from 1 to 5 MHz [14-15]. Shiiba et al. investigated spatial distrubution of cavitation in a 150 kHz sonoreactor and calculated BIV in the frequency range from 1 to 10 MHz [27]. However, in order to measure BIV accurately, it is necessary to completely eliminate a fundamental, all harmonic, all

subharmonic, and all ultraharmonic components in the frequency spectra.

There are several quatification methods of sonochemical intensity including Frickle [28], Weissler [29, 30], hydrogen peroxide [31, 32], sonochemical luminescence [20], phenolphtalein [33], porphyrin [34], rhodamin B [35], and potassium iodide (KI) [36, 37] methods. In Frickle and Weissler methods, carbon tetrachloride and strong acid are used, respectively. These chemicals have high toxicity. The concentration measurement of hydrogen peroxide in the solution is not simple. To detect sonochemical luminescence with high sensitivity, it needs to use a transparent reactor and gather luminescence from the whole reactor into a photodetector in a dark room. The reaction mechanism of phenolphtalein, porphyrin, and rhodamin B are complex. The KI solution has been used as a popular chemical dosimetry because it is safe to handle the solutions and the concentration measurement is easy. The KI method is the standard method for the estimation of sonochemical efficiency [37]. Under ultrasonic irradiation, an aluminum foil is pitted in the solution by shock waves and micro-jet generated from the collapse of bubbles. It is possible to determine the mechanical effect threshold by observation of the erosion on the surface of aluminum foil by ultrasounic irradiation [22].

The measurement of cavitation threshold has been mainly conducted below frequency of 100 kHz used for the cleaner and homogenizer. Threshold data in the frequency range from 100 kHz to 1 MHz are important for sonochemical reactor because the performance of sonochemical reaction is high [37]. However, cavitation threshold for this frequency range are few reported. Moreover, thresholds of chemical effect and mechanical effect have been still insufficientltly investigated and these data are greately lesser than cavitation threshold data.

The objective of this study is clarifying the frequency dependence of the cavitation, chemical effect, and mechanical effect thresholds in the wide frequency range from 22 to 4880 kHz. The cavitation, chemical effect, and mechanical effect thresholds were determined by broadband noise, KI oxidation, and aluminum foil erosion, respectively. In the measurement of cavitation threshold, the fundamental, all harmonic, all subharmonic, and all ultraharmonic components in the spectra were completely removed prior to integrating broadband noise and the integrating region was decided from 20 kHz to 20 MHz for all driving frequencies.

In addition, the sound pressures at the second harmonic and the first ultraharmonic frequencies in the spectra were measured for an indicator of bubble occurrence in water [13]. The minimum sound pressure amplitude required to emit the second harmonic and the first ultraharmonic components, that is, thresholds of the second harmonic and the first ultraharmonic signals were estimated.

2. Experimental

2.1. Apparatus

Figure 1 shows the setup of experimental apparatus. Driving ultrasonic frequencies were 22, 43, 98, 304, 488, 1000, 2000, and 4880 kHz. A stainless steel reactor with inner diameter of 56.8 mm was used for all experiments. A Langevin type transducer with multiple frequencies (HEC45242M, Honda Electronics) was used from 22 to 98 kHz and its diameter was 45 mm. Disc type transducers (Honda Electronics) with 50 mm in diameter were used for 304, 488, 1000, and 2000 kHz. A disc type transducer with 20 mm in diameter was used for 4880 kHz. The transducer was fixed at the bottom of the reactor. A cooling fan was attached to avoid heating the transducer. A circulating water bath was connected to the annular section of the reactor to maintain the sample temperature at 298 ± 1 K.

A signal generator (WF1974, NF) was used to generate a continuous sinusoidal wave signal. The signal was amplified by a power amplifier (1040L, E&I). An impedance matching circuit (Honda Electronics) was connected between the power amplifier and the transducer to match the impedance of transducer at 22, 43, 98, 1000, 2000, and 4880 kHz. The voltage at the both end of transducer and the current through the transducer were measured by an oscilloscope (TDS3014B, Tektronix) and a current probe (TCP202, Tektronix), respectively, and the effective electric power applied to the transducer was thereby calculated. The output waveform amplitude of signal generator was set by PC via a general purpose interface bus (GPIB). An electric control system (Honda Electronics) was used to set a constant electric power applied to the transducer.

To measure the sound pressure at a wide range of frequencies, the needle type hydrophone (HUS-200S, Honda Electronics) calibrated sound pressure in the frequency range from 20 kHz to 20 MHz was used. The hydrophone tip was located at the position where the highest sound pressure was received in the reactor by using a XYZ axis stage controller (SHOT-204, Sigmakoki). The hydrophone was connected to the spectrum analyzer (8595E, HP) accompanied by a preamplifier (Honda Electronics, HUS-200A) which converted impedance. To prevent hysteresis effect induced by acoustic cavitation, experiments were conducted by increasing electric power applied to the transducer [13, 38].

Air-saturated distilled water was used in all experiments. The sample volume was 0.100 dm^3. The sample was left at rest in the reactor for 30 minutes before measurement. After every experiment, the solution was changed to a fresh one for the next experiment. Each threshold value was measured three times.

2.2. Measurements

2.2.1. Broadband noise

The amount of generated acoustic cavitation was estimated by BIV calculated from broadband noise in the output voltage of the hydrophone. The signal spectra in the spectrum analyzer at 1000 kHz with the electric input power of 50 W and background noise are displayed in Fig. 2. BIV was calculated from the output voltage by the following equation,

$$\mathrm{BIV} = \int_{f_s}^{f_e} [V_S(f) - V_N(f)]\, df \qquad (1)$$

where $V_S(f)$ represents the output voltage received from the hydrophone after eliminating fundamental, all subharmonic, all harmonic, and all ultraharmonic components, and $V_N(f)$ represents the output voltage of the background noise as shown in Fig. 2. In this study, the start frequency of integration region, f_s, was at 20 kHz, and the stop frequency, f_e, was at 20 MHz. The hydrophone output voltage was expressed in decibels (dB) and was used to calculate the BIV denoted as the shaded area in Fig. 2.

2.2.2. KI oxidation

The chemical effect threshold was determined by KI oxidation method. When the ultrasound is irradiated to KI aqueous solution at a concentration of 0.1 mol·dm^{-3}, I^- ions are oxidized by OH radical, generating I_2. I_2 reacts with the excess I^- in the solution to form I_3^- ion by the next reaction,

$$I_2 + I^- \leftrightarrows I_3^- \qquad (2)$$

The concentration of I_3^- ions was measured by an ultraviolet spectrometer (UV-1600, Shimadzu) at 355 nm [37] using quartz cuvettes with the length of 5 cm. The reaction rate of KI oxidation was calculated by the following equation,

$$k = \frac{AW}{\varepsilon l t} \qquad (3)$$

where k is reaction rate (mol·s^{-1}), ε is the molar extinction coefficient of I_3^- (ε = 26,303 dm^3 mol^{-1} cm^{-1}), A is absorbance, l is the cuvette length (cm), W is the solution volume (dm^3), and t is sonication time (s). The irradiation time of ultrasound was 120 minutes.

2.2.3. Aluminum foil erosion

To determine mechanical effect threshold, the aluminum foil was pitted by ultrasonic irradiation in air-saturated water. The thickness, length, and width of an aluminum foil were 12 μm, 200 mm, and 50 mm, respectively. The surface of aluminum foil was placed perpendicular to the transducer surface and its center was located on the axis of the transducer center. The irradiation time of ultrasound was within 180 minutes.

3. Results and discussion

3.1. Cavitation threshold

In order to obtain resonance condition of water, ultrasonic frequency was adjusted to a minimum impedance of the transducer. Figure 3 shows the vertical distribution of hydrophone output voltage at fundamental frequency on the axis of the transducer center. The abscissa indicates the distance between the hydrophone and the transducer. The driving frequency and effective electrical power applied to the transducer are 43 kHz and 0.01 W, respectively. A standing wave is observed and the output voltage becomes the highest value when the hydrophone position is 33 mm. Experiments for determining cavitation threshold were carried out at the hydrophone position giving highest sound pressure for each driving frequency.

Figures 4 (a) and (b) show the sound pressure at the fundamental frequency and BIV against the square root of electric power at 98 kHz and 2000 kHz, respectively. The sound pressure is zero-to-peak amplitude. At low electric power in Fig. 4(a), the sound pressure increases linearly with increasing square root of electric power and BIV is almost zero. However, above the square root of electric power of 0.71 $W^{1/2}$, BIV increases and the sound pressure becomes unstable. This behavior means that acoustic cavitation starts to generate at 0.71 $W^{1/2}$. In order to obtain the cavitation threshold, the sound pressure is assumed to be proportional to the square root of electric power at high electric power. The sound pressure at 0.71 $W^{1/2}$ is regarded as the cavitation threshold as shown dotted lines. The cavitation threshold at 98 kHz is 71.4 kPa. The similar trend is also observed at 2000 kHz as shown in Fig. 4 (b). The averaged values of cavitation threshold at 22, 43, 98, 304, 488, 1000, 2000, and 4880 kHz are summarized in Table 1.

Figure 5 shows the dependence of cavitation threshold on the ultrasonic frequency. The cavitation threshold increases with increasing ultrasonic frequency. As the ultrasonic frequency increases, the duration of the rarefaction phase decreases because the pressure oscillation period decreases [39, 40]. Consequently, it becomes more difficult to occur cavitation bubbles. Therefore, in order to generate acoustic cavitation at high frequency, the high sound pressure is necessary.

The cavitation thresholds using broadband noise and bubble observation reported in

previous papers are also plotted in Fig. 5. Neppiras conducted broadband noise measurement and reported that cavitation threshold at 40 kHz was 27 kPa [10]. This value is close to the result of this research. However, he also reported that the cavitation threshold at 28 kHz was 84 kPa [11]. Barger showed that the cavitation threshold at 27 kHz was 42 kPa [41]. Hodnett and Zeqiri indicated that the cavitation threshold at 25 kHz was given as 82 kPa [12]. The existence of bubble nucleus originated from fine bubbles and roughness on surface of transducer and reactor might be a reason for the differences of cavitation thresholds. Gaete-Garreton et al. estimated cavitation threshold by numerical analysis and reported that cavitation threshold at 20 kHz was 30 kPa in the case of diameter of collapsing bubbles at 0.12 mm [22]. In the ultrasonic frequency range from 400 to 2000 kHz, Gabrielli and Iernetti conducted bubble observation by using a lateral light source [19]. The cavitation thresholds increased as the frequency became higher and their data are close to those in this study.

3.2 Thresholds of the second harmonic and the first ultraharmonic signals

As the sound pressure at the fundamental frequency increased in water, the sound signal at the second harmonic frequency (f_2) was not observed at first and it appeared above a certain threshold as shown in Fig. 2. The harmonic signals are mainly originated from nonlinear oscillations of stable bubbles in water [10]. However, the nonlinear propagation of sound influences the harmonic signal in megahertz range of ultrasound [42]. We defined the minimum sound pressure required to emit sound signal at the second harmonic frequency as the threshold of the second harmonic signal.

The sound signal at the first ultraharmonic ($f_{1.5}$) frequency also appeared above a certain sound pressure as shown in Fig. 2. The half-order subharmonic signals are mainly attributed to the sound waves from relatively large bubbles which oscillate with a doubled period of driving frequency [42]. From Fourier series of subharmonic components, the spectrum of any arbitrary periodic function is composed of the subharmonics and ultraharmonics for example the first ultraharmonic. The threshold of the first ultraharmonic signal was defined in the same way as threshold of the second harmonic. Thresholds of the second harmonic and the first ultraharmonic signals are shown in Table 1 and plotted against ultrasonic frequency in Fig. 5. The threshold of the second harmonic signal increases with increasing ultrasonic frequency in the frequency ranges of 22 - 488 kHz. This is because the low pressure period of ultrasound decreases at high frequency and it is difficult to generate stable bubbles. The threshold of the second harmonic signal approximates to the cavitation threshold below 1000 kHz. Above 1000 kHz, the threshold of the second harmonic

signal declines as the frequency increases because of the nonlinear propagation of sound.

The threshold of the first ultraharmonic signal gets higher along with increased ultrasonic frequency. Above 98 kHz, the threshold of the first ultraharmonic signal is close to the cavitation threshold. However, below 98 kHz, the threshold of the first ultraharmonic signal is higher than the cavitation threshold. At low ultrasonic frequency and low sound pressure, it might be difficult for large bubbles to trap at standing waves because of large buoyant force. At high sound pressure, large bubbles which oscillate with a doubled period of driving frequency are easily trapped at standing waves because primary Bjerknes force exceeds buoyant force. Therefore, the threshold of the first ultraharmonic signal is higher than the cavitation threshold at low ultrasonic frequency.

3.3. Threshold of chemical effect

OH radicals generated by the pyrolysis of water due to cavitation oxidize KI, I_3^- ion is formed by reaction (2) [43]. When cavitation is generated, OH radicals are released, that is why chemical effect is obtained in the solution. Figure 6 shows the effect of electric power on the reaction rate of I_3^- ion formation at 43 kHz. Below the electric input power of 2 W, the reaction rate is zero. Thereafter, the reaction rate increases with increasing electric power. It means that KI reaction starts to take place at the electric power of 2 W. From the linear relationship between the sound pressure at the fundamental frequency and the square root of electric power, the chemical effect threshold is obtained at 39.0 kPa. The chemical effect thresholds at all frequencies are summarized in Table 1.

Figure 7 indicates the dependence of chemical effect threshold on the ultrasonic frequency. The chemical effect threshold increases with increasing frequency. In conjunction with chemical effect threshold of this study, data of previous researches are also presented in Fig. 7. Yanagita *et al.* used luminol aqueous solution and measured the threshold of sonochemical luminescence [20]. The thresholds were obtained as 130 and 180 kPa at 1100 and 1700 kHz, respectively. Pickworth measured sonoluminescence from water and obtained the threshold value as 126 kPa at 1000 kHz [21]. These data seem to be in a good agreement with chemical effect threshold measured by KI oxidation in this study.

3.4. Threshold of mechanical effect

In order to estimate the mechanical effect threshold, erosion of aluminum foil was conducted by increasing electric power applied to the transducer. One example of erosion of aluminum foil by the mechanical effect of acoustic cavitation is displayed in Fig. 8. The driving frequency and electric power are 43 kHz and 1 W, respectively. The white part is the pit of aluminum foil. The

mechanical effect threshold is determined as the minimum sound pressure at the fundamental frequency which is capable of pitting aluminum foil. The mechanical effect threshold is obtained from the linear relationship between the sound pressure at the fundamental frequency and the square root of electric power and is shown in Table 1.

Figure 9 shows the dependence of mechanical effect threshold on the ultrasonic frequency. Erosion of aluminum foil by acoustic cavitation is observed from 22 kHz to 488 kHz. Above 1000 kHz, the aluminum foil is not eroded by ultrasound with the electric power applied to transducer of 100 W and irradiation time of 180 minutes. The mechanical effect threshold becomes higher as the ultrasonic frequency increases. Gaete-Garreton et al. performed the erosion of a thin aluminum film at 20 kHz [22]. The threshold of aluminum film erosion plotted in Fig. 9 seems to be close to the mechanical effect threshold in this study.

Kling and Hammitt [44] observed the damage of aluminum foil by cavitation bubbles. When the jet velocity generated by collapse of cavitation bubbles was 120 m/s, the aluminum foil with 50 μm of thickness was damaged. Wang and Manmi [45] simulated microbubble dynamics near a wall subject to high intensity ultrasound. The maximum bubble radius just before collapse and the jet velocity generated by the collapse of cavitation bubbles decreased as the frequency became higher. Mason and Lorimer [46] also reported that bubbles tended to be smaller by an increase of frequency and therefore their collapse was less violent. From these results, ultrasonic erosion at higher frequency needs higher sound pressure because the jet velocity decreases. That is why the mechanical effect threshold greatly increases with increasing frequency.

3.5. Comparisons of cavitation, chemical effect, and mechanical effect thresholds

The comparison of cavitation, chemical effect, and mechanical effect thresholds is shown in Fig. 10. With increasing frequency, all thresholds increase. The chemical effect threshold is close to the cavitation threshold on the wide range of frequency from 22 kHz to 4880 kHz. From this result, it is clear that the sonochemical reaction starts to occur almost at same condition for generation of acoustic cavitation. On the other hand, the mechanical effect threshold is nearly equal to the cavitation threshold at 22 and 43 kHz. However, in the range of ultrasonic frequency from 98 kHz to 488 kHz, mechanical effect threshold is much higher than cavitation and chemical effect thresholds. This is because the jet velocity generated by cavitation is low. The ultrasonic cleaner used the sound pressure range between cavitation threshold and mechanical effect threshold are effective for non-damage cleaning.

4. Conclusion

In this study, thresholds of cavitation, chemical effect, and mechanical effect from 22 kHz to 4880 kHz were determined by broadband noise, KI oxidation, and aluminum erosion methods, respectively. BIV was calculated from the broadband noise in the integration region from 20 kHz and 20 MHz for all frequencies. Before calculating, all fundamental, harmonic and subharmonic components were totally removed from signal spectrum. The results revealed a tendency of increasing thresholds of cavitation, chemical effect, and mechanical effect as ultrasonic frequency increased. The chemical effect threshold was shown to be close to the cavitation threshold on the whole range of frequency. The mechanical effect threshold was nearly equal to the cavitation threshold below 98 kHz, but greatly higher than the cavitation threshold at high frequency. Additionally, to detect the occurrence of bubbles in the liquid, the thresholds of the second harmonic and the first ultraharmonic components were measured. The threshold of the second harmonic and cavitation threshold were similar to each other below 1000 kHz. On the other hand, the threshold of the first ultraharmonic was higher than the cavitation threshold below 98 kHz and near to the cavitation threshold at high frequency.

References

1. M. D. Luque de Castro, F. Priego-Capote, Ultrasound-assisted crystallization (sonocrystallization), Ultrason. Sonochem. 14(6) (2007) 717-724.

2. B. Palanisamy, B. Paul, C. H. Chang, The synthesis of cadmium sulfide nanoplatelets using a novel continuous flow sonochemical reactor, Ultrason. Sonochem. 26 (2015) 452-460.

3. Z. Xu, K. Yasuda, Enhancement of sonochemical reaction by dual-pulse ultrasound, Jpn. J. Appl. Phys. 50 (2011) (07HE07-1-5).

4. T. Yotsumoto, T. Morita, Y. Noiri, Y. Kojima, Y. Asakura, S. Koda, Influence of pressure and temperature on sonochemical reaction in a flow-type reactor equipped with a PZT transducer, Jpn. J. Appl. Phys. 53(7S) (2014) (07KE09-1-3).

5. F. Martinez, A. Davidson, J. Anderson, S. Nakai, I. Desai, A. Radcliffe, Effects of ultrasonic homogenization of human milk on lipolysis, IgA, IgG, lactoferrin and bacterial content, Nutr. Res. 12 (1992) 561–568.

6. K. Yasuda, H. Honma, Z. Xu, Y. Asakura, S. Koda, Ultrasonic atomization amount for different frequencies, Jpn. J. Appl. Phys. 50(7S) (2011) (07HE23-1-5).

7. F. Chemat, Zill-e-Huma, M. K. Khan, Applications of ultrasound in food technology: processing, preservation and extraction, Ultrason. Sonochem. 18 (2011) 813–835.

8. J. Chandrapala, C. Oliver, S. Kentish, M. Ashokkumar, Ultrasonics in food processing, Ultrason. Sonochem. 19(5) (2012) 975-983.

9. C. D. Arvanitis, M. Bazan-Peregrino, B. Rifai, L. W. Seymour, C.-C. Coussios, Cavitation-enhanced extravasation for drug delivery, Ultrasound Med. Biol. 37(11) (2011) 1838-1852.

10. E. A. Neppiras, Measurement of acoustic cavitation, IEEE Trans. Sonics Ultrason. 15(2) (1968) 81-88.

11. E. A. Neppiras, Subharmonic and other low−frequency emission from bubbles in sound−irradiated liquids, J. Acoust. Soc. Am. 46(3B) (1969) 587-601.

12. M. Hodnett, B. Zeqiri, Toward a reference ultrasonic cavitation vessel: Part 2 - Investigating the spatial variation and acoustic pressure threshold of inertial cavitation in a 25 kHz ultrasound field**,** IEEE Trans. Ultrason. Ferroelectr. Freq. 55(8) (2008) 1809-1822.

13. J. Frohly, S. Labouret, C. Bruneel, I. Looten-Baquet, R. Torguet, Ultrasonic cavitation monitoring by acoustic noise power measurement, J. Acoust. Soc. Am. 108(5) (2000) 2012-2020.

14. T. Uchida, H. Sato, S. Takeuchi, T. Kikuchi, Investigation of output signal from cavitation sensor by dissolved oxygen level and sonochemical luminescence, Jpn. J. Appl. Phys. 49 (2010) (07HE03-1-2).

15. T. Uchida, S. Takeuchi, T. Kikuchi, Measurement of amount of generated acoustic cavitation: investigation of spatial distribution of acoustic cavitation generation using broadband integrated voltage, Jpn. J. Appl. Phys. 50 (2011) (07HE01-1-4).

16. H. B. Briggs, J. B. Johnson, W. P. Mason, Properties of liquids at high sound pressure, J. Acoust. Soc. Am. 19(4) (1947) 664-677.

17. M. B. Moffett, Cavitation thresholds of a polyalkylene glycol and of castor oil, J. Acoust. Soc. Am. 68(3) (1980) 966-969.

18. E. Meyer, Some new measurements on sonically induced cavitation, J. Acoust. Soc. Am. 29(1) (1957) 4-8.

19. I. Gabrielli, G. Iernetti, Cavitation and chemical effects in ultrasonic stationary fields, Acoustica. 13(3) (1963) 165-174.

20. H. Yanagida, Y. Masubuchi, K. Minagawa, J. I. Takimoto, K. Koyama, Effect of ultrasound frequency on sonochemical luminescence under well-determined sound pressure, Jpn. J. Appl. Phys. 38(5S) (1999) 3103-3104.

21. M. J. W. Pickworth, P. P. Dend, T. G. Leighton, A. J. Walton, Studies of the cavitational effects of clinical ultrasound by sonoluminescence: 2. Thresholds for sonoluminescence from a therapeutic ultrasound beam and the effect of temperature and duty cycle, Phys. Med. Biol. 33(11) (1988) 1249-1260.

22. L. Gaete-Garretón, Y. Vargas-Hernández, R. Vargas-Herrera, J. A. Gallego-Juárez, F. Montoya-Vitini, On the onset of transient cavitation in gassy liquids, J. Acoust. Soc. Am. 101(5) (1997) 2536-2540.

23. A. B. Michael, H. Inez, Impact of ultrasonic frequency on aqueous sonoluminescene and sonochemistry, J. Phys. Chem. A 105 (2001) 3796-3802.

24. T. J. Mason, A. J. Cobley, J. E. Graves, D. Morgan, New evidence for the inverse dependence of mechanical and chemical effects on the frequency of ultrasound, Ultrason. Sonochem. 18(2011) 226-230.

25. K. S. Suslick, The chemical effects of ultrasound, Sci. Am. 260(2) (1989) 80-86.

26. K. S. Suslick, J. M. Thomas, Ultrasonic Physical Mechanisms and Chemical Effects, in: K. S. Suslick, T. J. Matula, Wiley Encyclopedia of Electrical and Electronics Engineering, John Wiley & Sons, New York, 1999, pp. 647-657.

27. M. Shiiba, N. Kawashima, T. Uchida, T. Kikuchi, M. Kurosawa, S. Takeuchi, Estimation of cavitation sensor with hydrothermally synthesized lead zirconate titanate film on titanium cylindrical pipe: spatial distribution of acoustic cavitation field and basic characteristics of cavitation sensor, Jpn. J. Appl. Phys. 50(7S) (2011) (07HE02-1-5).
28. H. Fricke, E. J. Hart, The oxidation of Fe^{++} to Fe^{+++} by the irradiation with X-rays of solutions of ferrous sulfate in sulfuric acid, J. Chem. Phys. 30 (1935) 60-61.
29. T. Kimura, T. Sakamoto, J. M. Leveque, H. Sohmiya, M. Fujita, S. Ikeda, T. Ando, Standardization of ultrasonic power for sonochemical reaction, Ultrason. Sonochem. 3(3) (1996) S157-S161.
30. A. Weissler, H. W. Cooper, S. Snyder, Chemical effect of ultrasonic waves: oxidation of potassium iodide solution by carbon tetrachloride, J. Am. Chem. Soc. 72(4) (1950) 1769-1775.
31. O. Lindström, Physico‐chemical aspects of chemically active ultrasonic cavitation in aqueous solutions, J. Acoust. Soc. Am. 27(4) (1955) 654-671.
32. M. Sato, H. Itoh, T. Fujii, Frequency dependence of H_2O_2 generation from distilled water, Ultrasonics 38(1) (2000) 312-315.
33. L. Rong, Y. Kojima, S. Koda, H. Nomura, Simple quantification of ultrasonic intensity using aqueous solution of phenolphthalein, Ultrason. Sonochem. 8(1) (2001) 11-15.
34. H. Nomura, S. Koda, K. Yasuda, Y. Kojima, Quantification of ultrasonic intensity based on the decomposition reaction of porphyrin, Ultrason. Sonochem. 3(3) (1996) S153-S156.
35. M. Sivakumar, A. B. Pandit, Ultrasound enhanced degradation of Rhodamine B: optimization with power density, Ultrason. Sonochem. 8(3) (2001) 233-240.
36. E. J. Hart, A. Henglein, Free radical and free atom reactions in the sonolysis of aqueous iodide and formate solutions, J. Phys. Chem. 89(20) (1985) 4342-4347.
37. S. Koda, T. Kimura, T. Kondo, H. Mitome, A standard method to calibrate sonochemical efficiency of an individual reaction system, Ultrason. Sonochem. 10(3) (2003) 149-156.
38. E. A. Neppiras, Acoustic cavitation, Phys. Rep. 61(3) (1980) 159-251.
39. F. Grieser, P. –K. Choi, N. Enomoto, H. Harada, K. Okitsu, K. Yasui, Sonochemistry and the Acoustic Bubbles, Elsevier, 2015, pp. 41-83.
40. C. Pétrier, A. Francony, Ultrasonic waste-water treatment: incidence of ultrasonic frequency on the rate of phenol and carbon tetrachloride degradation, Ultrason. Sonochem. 4(4) (1997) 295-300.
41. J. Barger, Acoust. Res. Lab., Harvard Univ., Tech. Mem. No. 57 (April 1964).

42. K. Yasui, T. Tuziuti, J. Lee, T. Kozuka, A. Towata, Y. Iida, Numerical simulations of acoustic cavitation noise with the temporal fluctuation in the number of bubbles, Ultrason. Sonochem. 17(2) (2010) 460-472.
43. S. Merouani, O. Hamdaoui, F. Saoudi, M. Chiha, Influence of experimental parameters on sonochemistry dosimetries: KI oxidation, Fricke reaction and H_2O_2 production, J. Hazard. Mater. 178(1) (2010) 1007-1014.
44. C. L. Kling, F. G. Hammitt, A photographic study of spark-induced cavitation bubble collapse, J. Basic Eng. 94(4) (1972) 825-832.
45. Q. X. Wang, K. Manmi, Three dimensional microbubble dynamics near a wall subject to high intensity ultrasound, Phys. Fluids 26(3) (2014) (032104-1-23).
46. T. J. Mason, J. P. Lorimer, Theory, Applications and Uses of Ultrasound in Chemistry, Ellis Harwood Limited, John Wiley, New York (1988).

Figure captions

Fig. 1. Setup of experimental apparatus.

Fig. 2. Signal spectra in the spectrum analyzer at 1000 kHz and 50 W.

Fig. 3. Vertical distribution of hydrophone output voltage at fundamental frequency on the axis of transducer center at 43 kHz and 0.01 W.

Fig. 4. Sound pressure at fundamental frequency and BIV against the square root of electric power at (a) 98 kHz and (b) 2000 kHz.

Fig. 5. Dependence of cavitation threshold on ultrasonic frequency.

Fig. 6. Effect of electric power on reaction rate of I_3^- ion formation at 43 kHz.

Fig. 7. Dependence of chemical effect threshold on ultrasonic frequency.

Fig. 8. Aluminum foil erosion at 43 kHz and 1 W.

Fig. 9. Dependence of mechanical effect threshold on ultrasonic frequency.

Fig. 10. Comparison of cavitation, chemical effect, and mechanical effect thresholds.

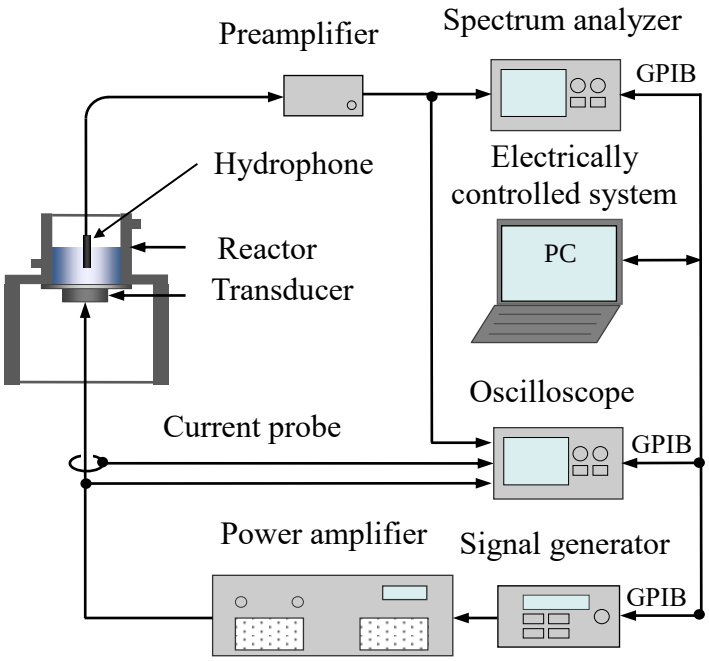
Preamplifier
Spectrum analyzer
GPIB
Hydrophone
Electrically
controlled system
Reactor
Transducer
PC
Oscilloscope
Current probe
GPIB
Power amplifier
Signal generator
GPIB

Fig. 1.

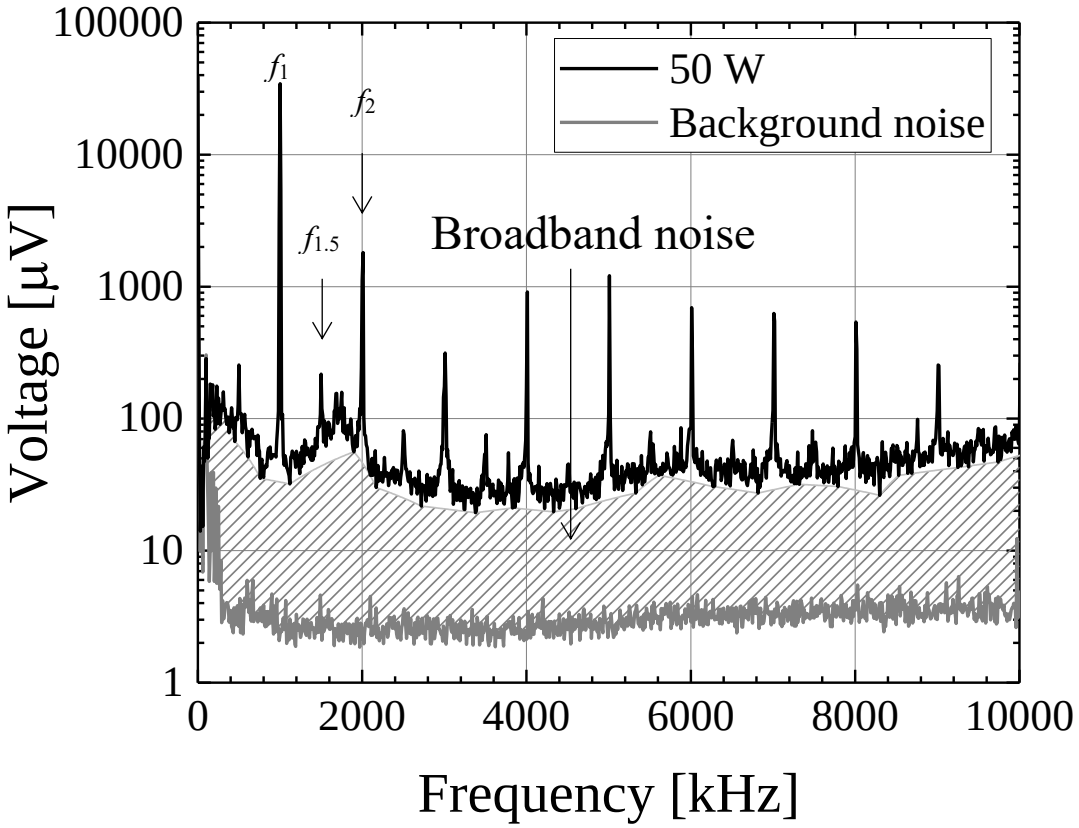
100000
10000
1000
100
10
1
Voltage [μV]
0
2000
4000
6000
8000
10000
Frequency [kHz]
50 W
Background noise
Broadband noise
f1
f2
f1.5

Fig. 2.

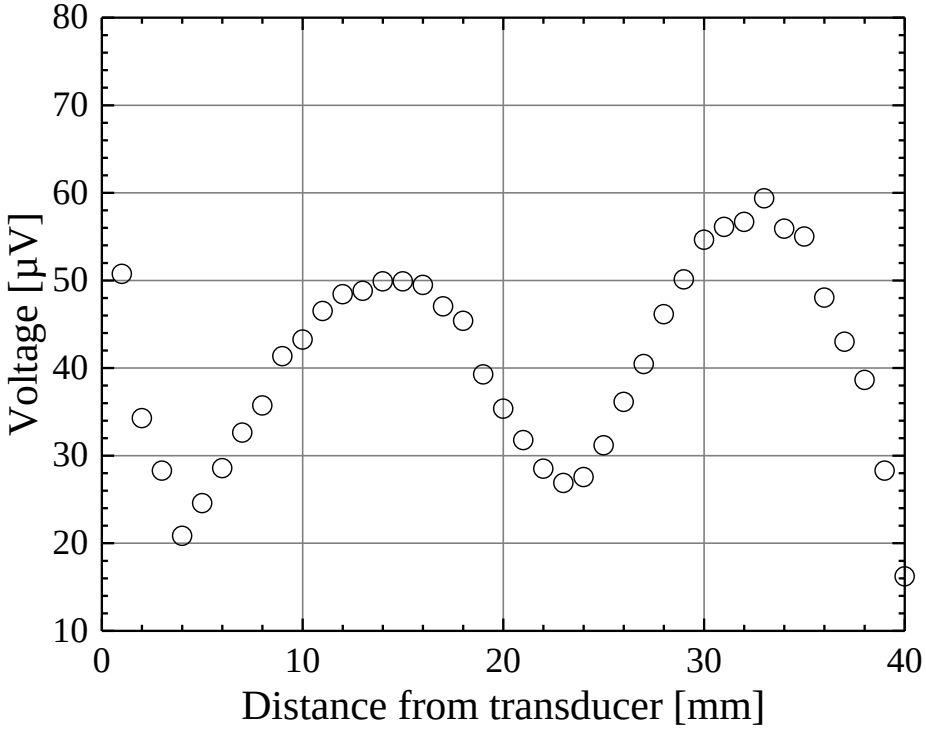
80
70
60
50
40
30
20
10
Voltage [µV]
0
10
20
30
40
Distance from transducer [mm]

Fig. 3.

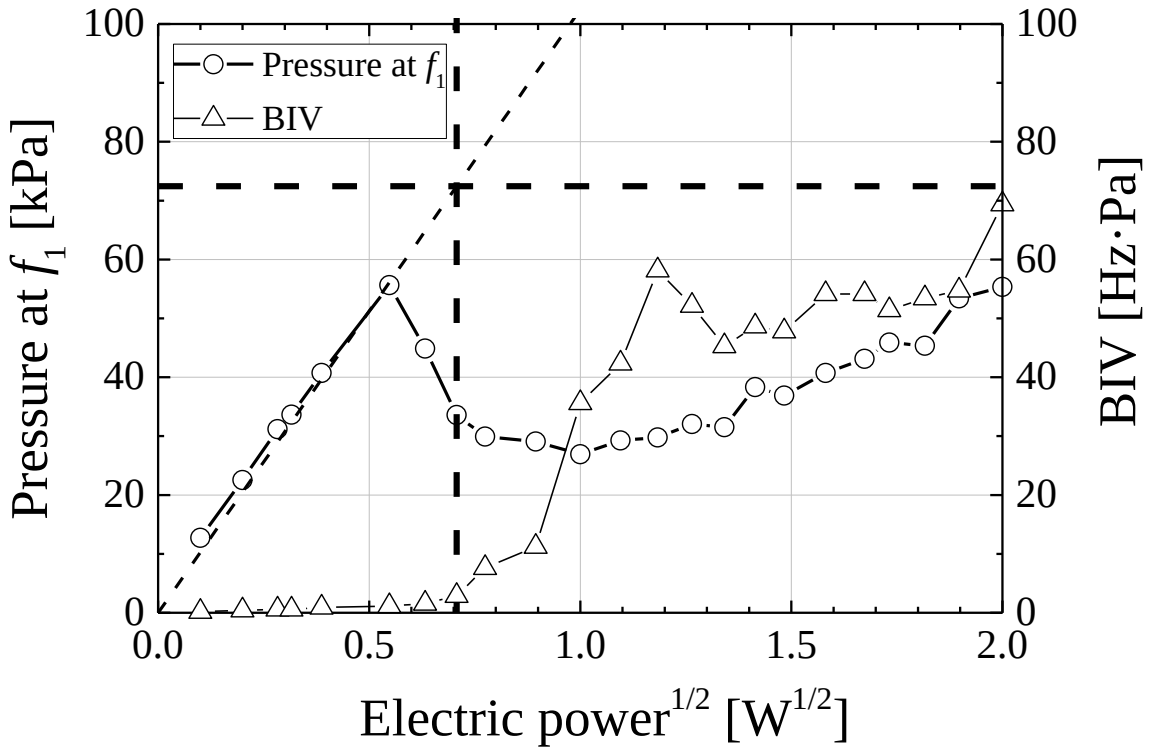
Pressure at f_1
BIV
Pressure at f_1 [kPa]
BIV [Hz·Pa]
Electric power$^{1/2}$ [W$^{1/2}$]
0
20
40
60
80
100
0.0
0.5
1.0
1.5
2.0

Fig. 4 (a)

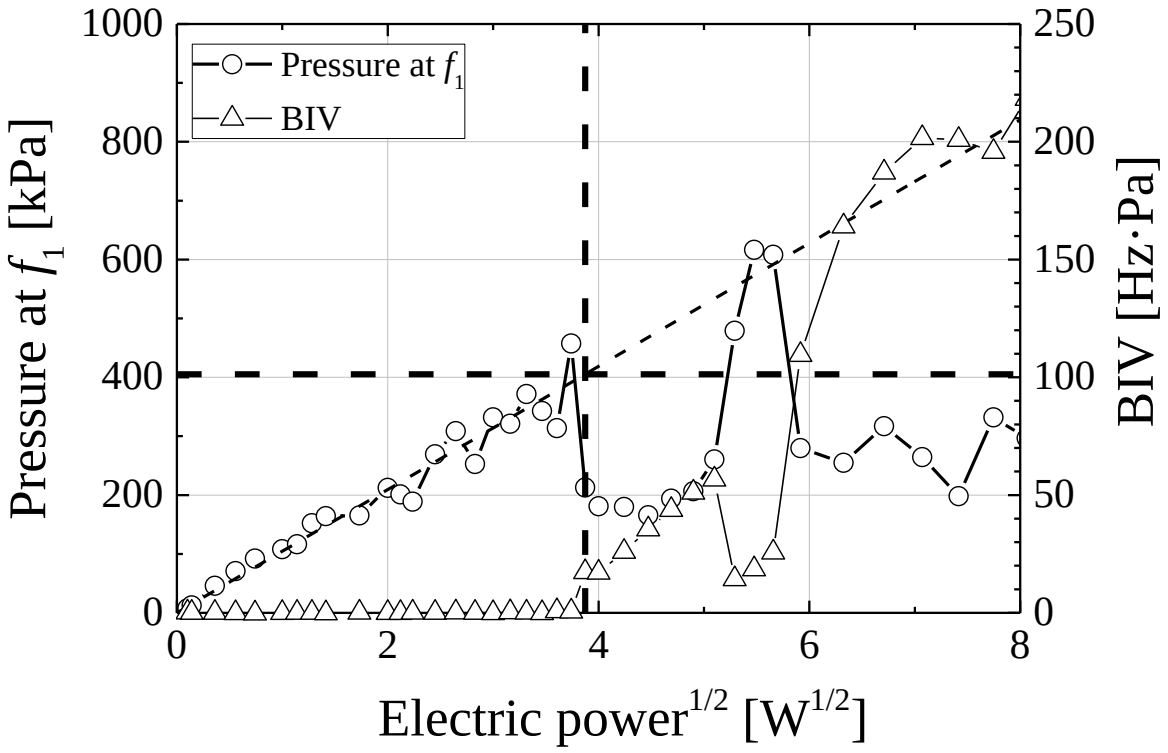
Pressure at f_1
BIV
Pressure at f_1 [kPa]
BIV [Hz·Pa]
Electric power$^{1/2}$ [W$^{1/2}$]
0
200
400
600
800
1000
0
50
100
150
200
250
0
2
4
6
8

Fig. 4 (b)

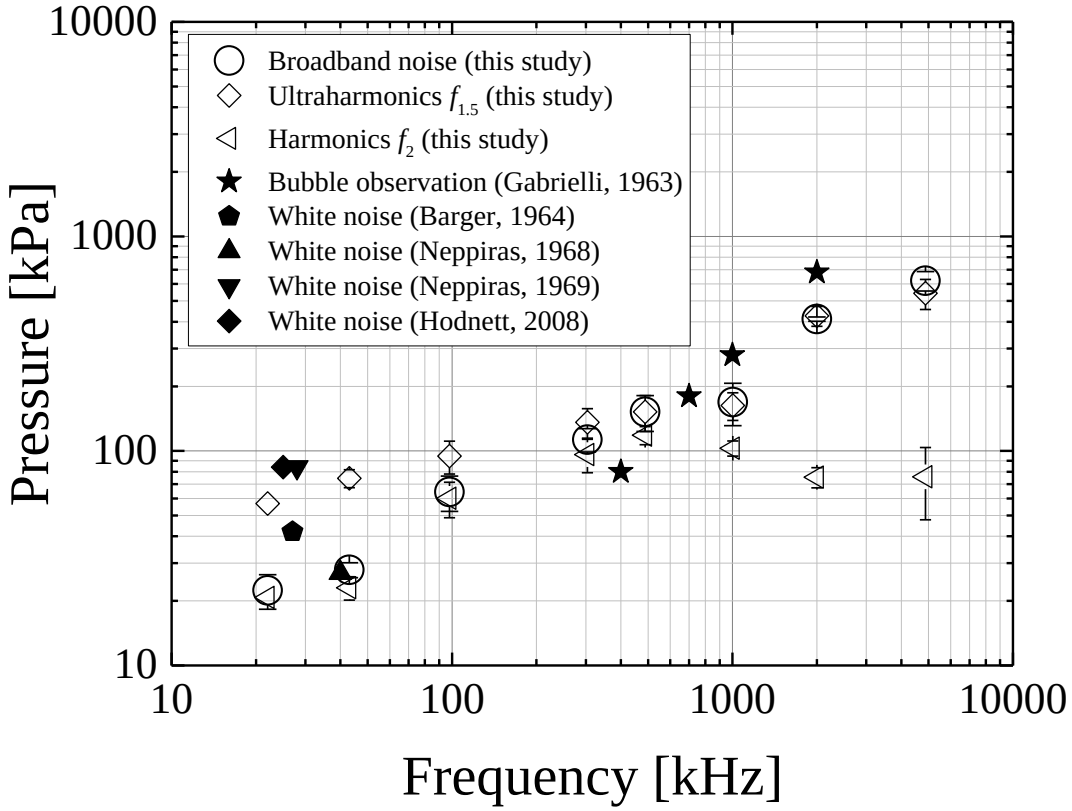
Broadband noise (this study)
Ultraharmonics $f_{1.5}$ (this study)
Harmonics f_2 (this study)
Bubble observation (Gabrielli, 1963)
White noise (Barger, 1964)
White noise (Neppiras, 1968)
White noise (Neppiras, 1969)
White noise (Hodnett, 2008)
Pressure [kPa]
10000
1000
100
10
10
100
1000
10000
Frequency [kHz]

Fig. 5.

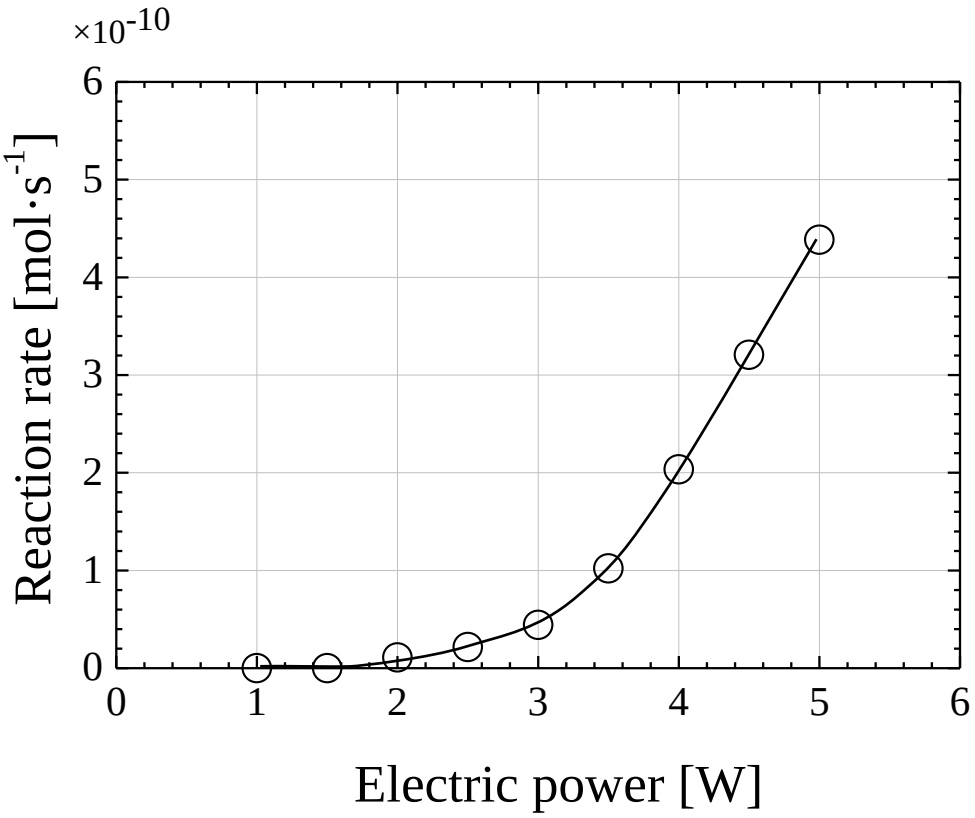

Fig. 6.

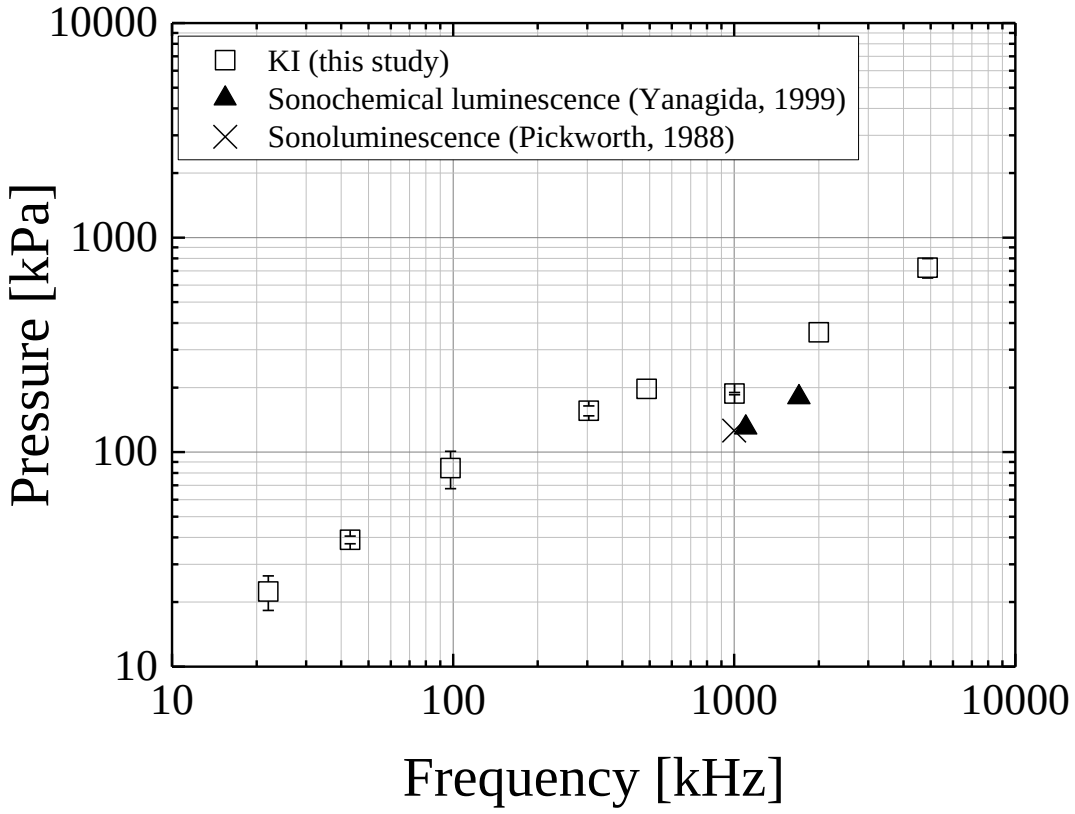
KI (this study)
Sonochemical luminescence (Yanagida, 1999)
Sonoluminescence (Pickworth, 1988)
Pressure [kPa]
10000
1000
100
10
10
100
1000
10000
Frequency [kHz]

Fig. 7.

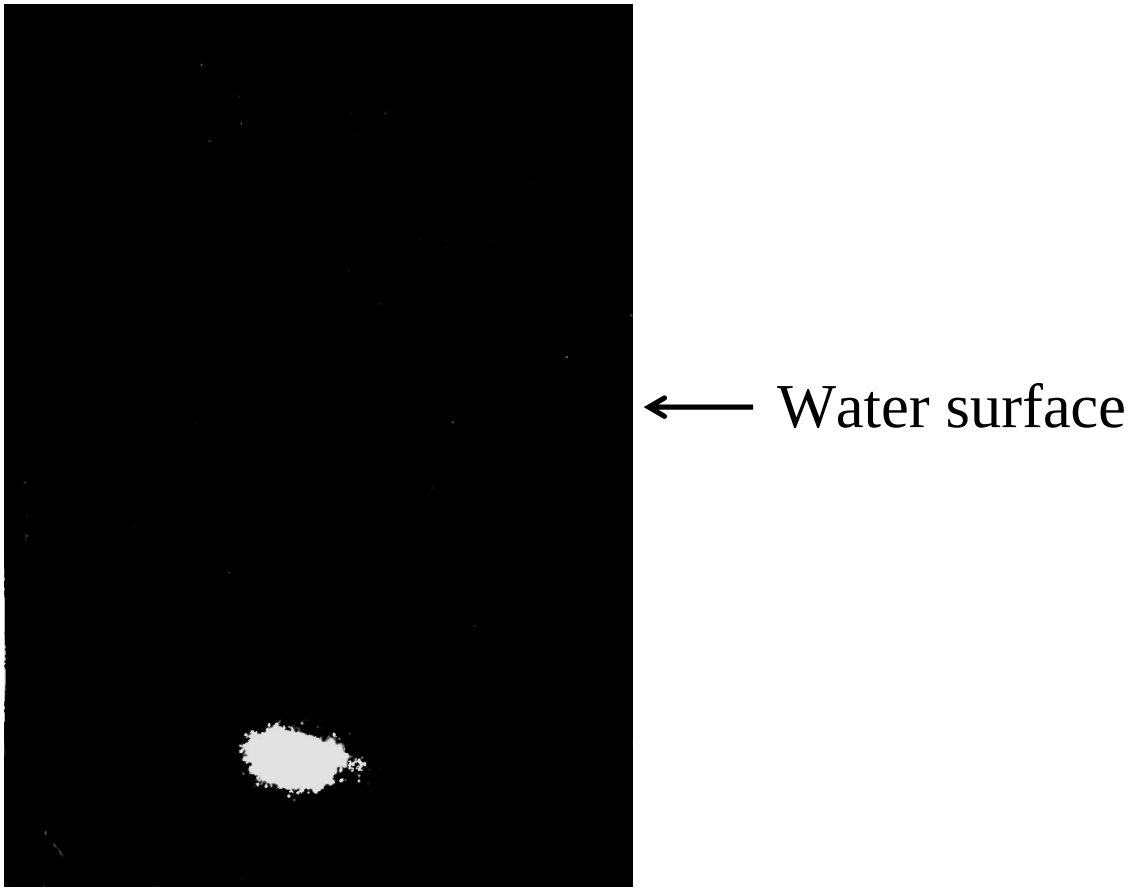

Fig. 8.

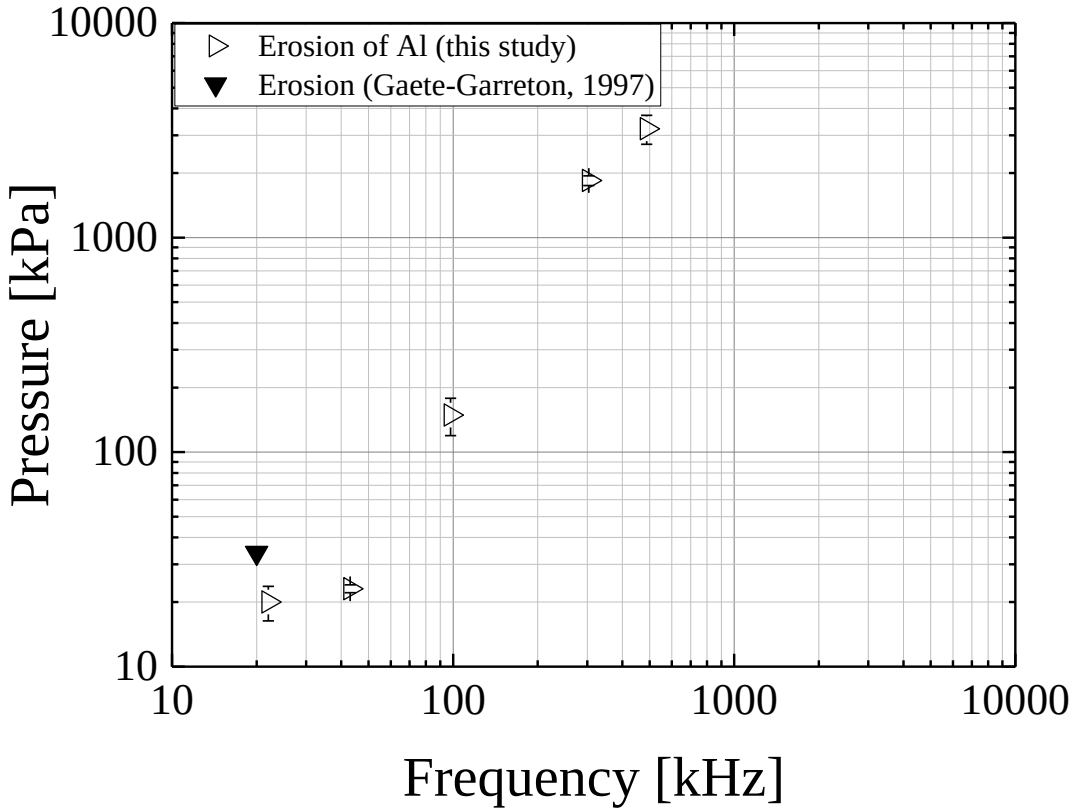
Erosion of Al (this study)
Erosion (Gaete-Garreton, 1997)
Pressure [kPa]
10000
1000
100
10
10
100
1000
10000
Frequency [kHz]

Fig. 9.

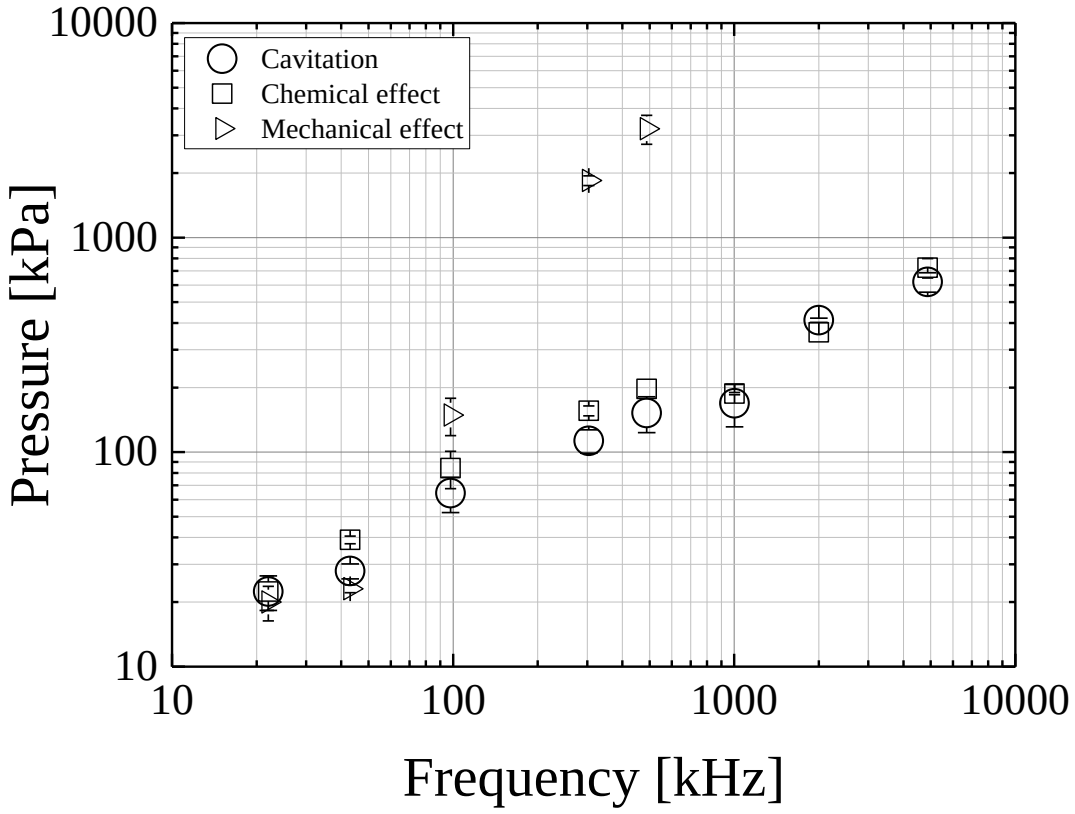
Cavitation
Chemical effect
Mechanical effect
Pressure [kPa]
Frequency [kHz]
10000
1000
100
10
10
100
1000
10000

Fig. 10.

Table 1. Thresholds of cavitation, chemical effect, mechanical effect, first ultraharmonic, and second harmonic

Frequency [kHz]	Cavitation [kPa]	Ultraharmonic $f_{1.5}$ [kPa]	Harmonic f_2 [kPa]	Chemical effect [kPa]	Mechanical effect [kPa]
22	22.4	56.9	20.8	22.4	20.0
43	27.9	74.5	23.0	39.0	23.1
98	63.7	94.6	60.1	84.2	149
304	113	136	96.2	156	1840
488	152	152	118	197	3220
1000	169	163	103	188	
2000	412	426	75.5	362	
4800	621	543	75.8	723	